https://doi.org/10.15407/knit2023.01.003
UDC 528.88; 528.852+845:519.237.8:004.93

YA. I. ZYELYK, Principal Researcher, Dr. Sci. in Tech., Senior Researcher
S. V. CHORNYY, Senior Researcher, PhD. in Tech., Associate Professor
O. P. FEDOROV, Director, Head of Department, Corresponding Member of the National Academy of Sciences of Ukraine, Dr.Sci. in Phys. & Math., Honored Worker of Science and Technology of Ukraine, Winner of State Awards in Science and Technology of Ukraine, Corresponding Member of the IAA
L. V. PIDGORODETSKA, Senior Researcher, PhD. in Tech.
E-mail: pidgorodetska@ukr.net
L. M. KOLOS, Senior Researcher, PhD. in Tech.

Space Research Institute National Academy of Sciences of Ukraine and State Space Agency of Ukraine
40 Academician Glushkov Ave., build. 4/1, Kyiv 187, 03187 Ukraine

SPATIAL RESOLUTION ENHANCEMENT OF THE LAND SURFACE THERMAL FIELD IMAGERY BASED ON MULTIPLE REGRESSION MODELS ON MULTISPECTRAL DATA FROM VARIOUS SPACE SYSTEMS

The methodology has been developed for enhancing the spatial resolution of the land surface thermal field satellite imagery based on the following steps: coupling images in the visible, thermal, and radar ranges into the single multispectral data product; constructing regression models of the images' relationship; performing the linear regression of the pseudo-thermal product with enhanced spatial resolution from the visible and radar ranges data. The methodology is implemented on the Google Earth Engine open cloud platform using the Earth Engine API and the software scripts created in the JavaScript language with the processing of multispectral image collections of various space systems at specified time intervals.

The possibility of practical synthesis of the pseudo-thermal image with an enhanced spatial resolution of 10 m based on the thermal image with the resolution of 100 m and the multispectral composite with the layers' resolution of 10 m and 30 m is shown.

The technology has been developed for synthesis and calibration of the land surface temperature product with enhanced spatial resolution and daily data providing rate based on the brightness temperature product in the B10 band of Landsat 8 and linear regression on the MODIS, ASTER, and Sentinel 1 products with daily to moderate data providing rates. The software in JavaScript has been developed, and technology has been implemented in the interactive web service form with open access on the Google Earth Engine Apps cloud platform.

The final data product provides the satisfactory relative root mean square error of the brightness temperature recovery of not more than 6 % according to the reference cross-calibration data of the B10 Landsat 8 band in the moderate thermal field (up to 100° C). The relative root mean square errors of the synthesized data according to the reference data on high-temperature sites (fire, hot lava) up to 28 % are due to the fact that the synthesized product contains information from high-temperature spectral bands (B07-B09 from ASTER), while the reference product (B10 from Landsat 8) does not contain such information.

Technology implementation examples show that cross-calibration of the synthesized product can be performed during the year from March to October according to reference thermal images of natural or artificial objects. Objects selected for calibration must have stable thermal characteristics at the time of the satellite flight during the data acquisition period.

Keywords: *land surface temperature, brightness temperature, space resolution of imagery, multiply linear regression, heterogeneous multispectral data coupling, data providing rate, product cross-calibration, Google Earth Engine.*

Цитування: Zyelyk Ya. I., Chornyy S. V., Fedorov O. P., Pidgorodetska L. V., Kolos L. M. Spatial resolution enhancement of the land surface thermal field imagery based on multiple regression models on multispectral data from various space systems. *Space Science and Technology.* 2023. **29**, № 1 (140). P. 03—14. https://doi.org/10.15407/knit2023.01.003

The problem of the land surface thermal field remote sensing, the idea and objectives of the study. A sufficiently detailed review of the problem statement of the land surface thermal field satellite monitoring and methods of its solution was carried out in [3, 6]. Among the many known methods for remote land surface temperature estimation, the single-channel methods are the most common. In particular, they are used in space systems with one infrared thermal channel of the Landsat series. When implementing the single-channel method, the spectral density of radiance in the thermal infrared channel is usually converted into the effective brightness temperature at the sensor aperture by inversion of Planck's law of thermal radiation [2, 4—6]. In turn, the spectral density of radiance at the sensor aperture in each thermal infrared channel is calculated through the processing level 1 data product, i.e., digital numbers of pixels, using coefficients of radiometric calibration, which are contained in the image metadata file. Further, the effective brightness temperature at the sensor aperture is converted into the thermodynamic temperature of the land surface using the thermal emissivity values. The thermal emissivity is estimated using satellite data of the optical radiation range of processing level 2: based on the land cover classification according to spectral reflectance for specific land cover classes [2, 4—6] or each pixel based on the determination of the normalized differential vegetation index (*NDVI*) of the land cover [3]. Thus, the retrieving of the land surface temperature according to thermal infrared channels data with low resolution using the optical range data with substantially higher resolution allows us, ultimately, to enhance the spatial resolution of the thermal field imagery.

However, the spatial resolution of the thermal field imagery of the land surface can be enhanced also at the processing level 1 of the primary data product, i.e., digital pixel numbers of the thermal infrared channels rasters. The idea of the spatial resolution enhancement of the thermal field imagery just in this way is expressed in [4]. The satellite data in the visible, thermal, and radar ranges from various space systems are coupled into the single multispectral data product of processing level 1, represented by the digital numbers of pixels in each raster layer. Based on the study of physical relationships between the fields of thermal, visible, and radar ranges, mathematical models of their relationship can be constructed, which are based on the laws of energy balance, heat transfer, and others. In particular, regression models of functional dependencies between digital numbers of pixel images in the thermal infrared range and the visible and radar radiation ranges are constructed. As a result of the implementation of the regression procedure constructed in this way on the selected land surface area, the synthesized pseudo-thermal image will have an increased spatial resolution. It is determined by the best spatial resolution of the raster layer of the coupled multispectral data product, i.e., the image in the radar range or visible range among those involved in the regression.

Thus, one of the objectives of the present study is the methodology development and implementation for enhancement of the spatial resolution of the land surface thermal field satellite imagery based on the following steps: coupling images in the visible, thermal, and radar ranges into the single multispectral data product; constructing of regression models of the images' relationship; performing the linear regression of the pseudo-thermal product with enhanced spatial resolution on the visible and radar ranges data.

The second objective of the study is related to the need to synthesize the product of the land surface temperature, which, unlike existing temperature products, would combine the enhanced spatial resolution and high data providing rate (daily). Such a pseudo-temperature product can be constructed based on the product of the B10 Landsat 8 thermal infrared channel (as a reference), converted to radiation temperature, and linear regression according to the proposed methodology on data of other space systems with different data providing rates.

Therefore, the second study objective is the technology development and implementation for synthesis and calibration of the land surface temperature product with the enhanced spatial resolution with daily data providing rate based on the brightness temperature in the B10 Landsat 8 channel and linear regression on products of other space systems with data providing rate from daily to moderate.

Methodology for the spatial resolution enhancement of the land surface thermal field satellite imagery

based on regression models on multispectral data from different space systems. Based on the laws of heat balance and heat transfer for the pixels of rasters in the channels of the constructed multispectral composite, the equations are obtained which characterize the relationship between the pixel values of the thermal infrared and visible radiation ranges. With steady-state heat transfer mode for the absolute thermodynamic temperature T of the land surface area, corresponding to each pixel of the image in the thermal infrared channel, the following equation is valid:

$$T = T_0 + (k_{abs} / c) \cdot W_{abs} - (k_{diss} / c) \cdot W_{diss}, \quad (1)$$

where c is the specific heat capacity, T_0 is the absolute temperature of the external environment, k_{abs} is thermal absorption, W_{abs} is the absorbed energy from the Sun's radiation and other factors, k_{diss} is thermal emissivity, and W_{diss} is the energy emitted by the land surface area. From (1) it follows the linear regression dependence for the absolute thermodynamic temperature T of the land surface pixel from the absorbed energy W_{abs}:

$$T = G \cdot W_{abs} + B, \quad (2)$$

where the coefficients G and B have the following form:

$$G = k_{abs} / c,$$

$$B = T_0 - (k_{diss} / c) \cdot W_{diss}.$$

Similar to (2) for digital numbers of the pixel of the brightness temperature T^{ir} at a sensor, taking into account the fact that the single pixel in the thermal infrared range is covered by the set of $i = \overline{1,n}$ pixels with digital numbers DNI_i^{vis} in the panchromatic range, and a fact that $DNI_i^{vis} = f(W_{abs})$, one obtains the following regression equation of the relationship between the digital numbers of the pixel in the thermal infrared and visible radiation ranges:

$$T^{ir} = \sum_{i=1}^{n} (G_i^{rad} \cdot DNI_i^{vis} + B_i^{rad}). \quad (3)$$

Based on (3), the calibration coefficients G_i^{rad}, B_i^{rad} are determined from the following equations system for the cross-calibration of the spectral channels in the coupled multispectral composite:

$$T_p^{\ ir} = \sum_{i=1}^{n} (G_i^{rad} \cdot DNI_{ip}^{vis} + B_i^{rad}), \quad (4)$$

$$p = \overline{1,m}; m \geq n.$$

The linear multiple regression coefficients and product of the land surface temperature with the enhanced spatial resolution are determined on the basis of the (4) type equation system, extended to the case of involving the radar range data in the regression. The procedure for the (4) type equation system solution is implemented on the cloud computing platform Google Earth Engine using classifiers' functions in a linear regression mode or linear regression reducers functions [5, 6]. The classifier in the linear regression mode is trained on the pixel set of the thermal infrared band layer with a low spatial resolution. The output of the classifier in linear regression mode is the raster of the synthesized pseudo-thermal image with the enhanced spatial resolution, constructed on the basis of the thermal image of the same land site with the low spatial resolution. The enhanced spatial resolution of the synthesized pseudo-thermal image is determined by the best spatial resolution of the raster layer of the coupled multispectral data product, i. e., an image in the radar range or visible range among those involved in the regression.

The data processing stages in the methodology implementation are as follows:

- Creating the image collection from various space systems for joint processing (attribute fields are satellites, region, and time interval). When the processing time interval is set to 1 month, the collection of multispectral images is formed, containing 1-2 Landsat 8 images (OLI, TIRS), several dozen Sentinel 2 images, and more than a hundred Sentinel 1 radar images.
- Creating the single multispectral image composite with the resulting single projection and the single highest spatial resolution among all layers.
- Regression of the pseudo-thermal image with the enhanced spatial resolution on the data of the visible radiation range, and, when involving radar data in the coupling procedure, additional regression on the data of the radar range with the high spatial resolution.
- Classifier training in the linear regression mode, i.e., the determination of linear regression coefficients, which is carried out on the initial data of the thermal infrared range of a low spatial resolution.
- Validation of the output pseudo-thermal image on the independent validation data set. Three classifiers in the regression mode in GEE have been stud-

ied in relation to the aimed task: gmoLinearRegression, svm, minimumDistance.

• The final stage of data processing is the calibration of the average value of the output pseudo-thermal image with the enhanced spatial resolution on a similar value of the input image in the thermal infrared range with a low spatial resolution.

The methodology is implemented on the Google Earth Engine open cloud platform using the Earth Engine API and the software scripts created in the JavaScript language for the processing of multispectral image collections of various space systems at specified time intervals.

The methodology implementation and testing. The considered methodology for the land surface thermal field spatial resolution enhancement has been tested on the monitoring examples of the thermodynamic temperature of peat lands, wild fires, and volcanoes. The studies used data from satellite sensors in the visible, thermal, and radar ranges for the three options of the space systems' grouping: I. Sentinel 1, Sentinel 2, and Landsat 8; II. Sentinel 1 and Landsat 8; III. Sentinel 1 and Terra/ASTER.

In option I, the classifier input in the regression mode is the multispectral composite image in the next channels with the corresponding spatial resolution: Sentinel 1: *VV*, *VH* (polarization) — 10 m; Sentinel 2: $B_2...B_4$, B_8 — 10 m, B_{11}, B_{12} — 20 m; Landsat 8: B_{10} — 30 m after resampling from 100 m. The classifier output in the regression mode is the single-layer pseudo-thermal image T_I^{ir} with the enhanced spatial resolution of 10 m, corresponding to the spatial resolution of the Sentinel 1 data and satisfying the regression equation:

$$T_I^{ir} = g_{VV} \cdot VV + g_{VH} \cdot VH + \sum_{i=2}^{3,4,8,11,12} g_{Bi} \cdot B_i + L_I^0 , \quad (5)$$

$$(i = 2, 3, 4, 8, 11, 12),$$

where g_{VV}, g_{VH}, g_{Bi}, L_I^0 are linear regression coefficients (L_I^0 is the offset coefficient).

In option II, the input of the classifier in the regression mode is the multispectral composite image in the next channels with the corresponding spatial resolution: Sentinel 1: *VV*, *VH* — 10 m; Landsat 8: B_6, B_7 — 30 m, B_8 — 15 m, B_{10} — 30 m. The classifier output in the regression mode is the pseudo-thermal image T_{II}^{ir} with the spatial resolution of 10 m:

$$T_{II}^{ir} = g_{VV} \cdot VV + g_{VH} \cdot VH + \sum_{i=6}^{8} g_{Bi} \cdot B_i + L_{II}^0 , \quad (6)$$

$$(i = 6, 7, 8),$$

where g_{VV}, g_{VH}, g_{Bi}, L_{II}^0 are linear regression coefficients (L_{II}^0 is the offset coefficient).

In option III, the input of the classifier in the regression mode is the multispectral composite image in the next channels with the corresponding spatial resolution: Sentinel 1: *VV*, *VH* with the resolution of 10 m; Terra/ASTER: $B_1...B_{3N}$ with the resolution of 15 m, B_4 with the resolution of 30 m, *median*(B_5, ..., B_9) is the single layer of the pixel values, which are the corresponding median pixel values in the (B_5, ..., B_9) channels, with the resolution of 30 m, $B_{10}...$ B_{14} are the thermal channels with the resolution of 90 m. The classifier output in the regression mode is the pseudo-thermal image T_{III}^{ir} with the spatial resolution of 10 m:

$$T_{III}^{ir} = g_{VV} \cdot VV + g_{VH} \cdot VH + \sum_{i=1}^{4} g_{Bi} \cdot B_i +$$

$$+\text{median}\,(B_5,\ldots, B_9) + \sum_{j=10}^{14} g_{Bj} \cdot B_j + L_{III}^0 ,$$

$$(i = \overline{1, 4};\ j = \overline{10, 14}),$$

where g_{VV}, g_{VH}, g_{Bi}, L_{III}^0 are linear regression coefficients (L_{III}^0 is the offset coefficient).

Fig. 1 shows fragments of the brightness temperature raster in the thermal infrared channel B_{10} Landsat 8 TIRS (the spatial resolution is 100 m) and a synthesized pseudo-thermal image T_I^{ir} with the enhanced spatial resolution 10 m according to the regression model (5) on the background of Google map for the selected object of the company's petroleum storage depot "BRSM-Nafta" in the Vasylkiv district of the Kyiv region before the fire and on the fire date June 9, 2015, respectively. The upper limit of the brightness temperature scale of 100 °C is explained by the saturation of the 16-bit ADC in the B_{10} channel of Landsat 8 TIRS at $T_{\max}^{br} = 94.88$ °C.

In the considered example, to create multispectral composites and regression equations constructed for classifier training, collections of images were formed before the fire from 1 to 30 May 2015 and during the fire from 9 to 19 May 2015 from sensors of various space systems with different spatial resolutions: Sen-

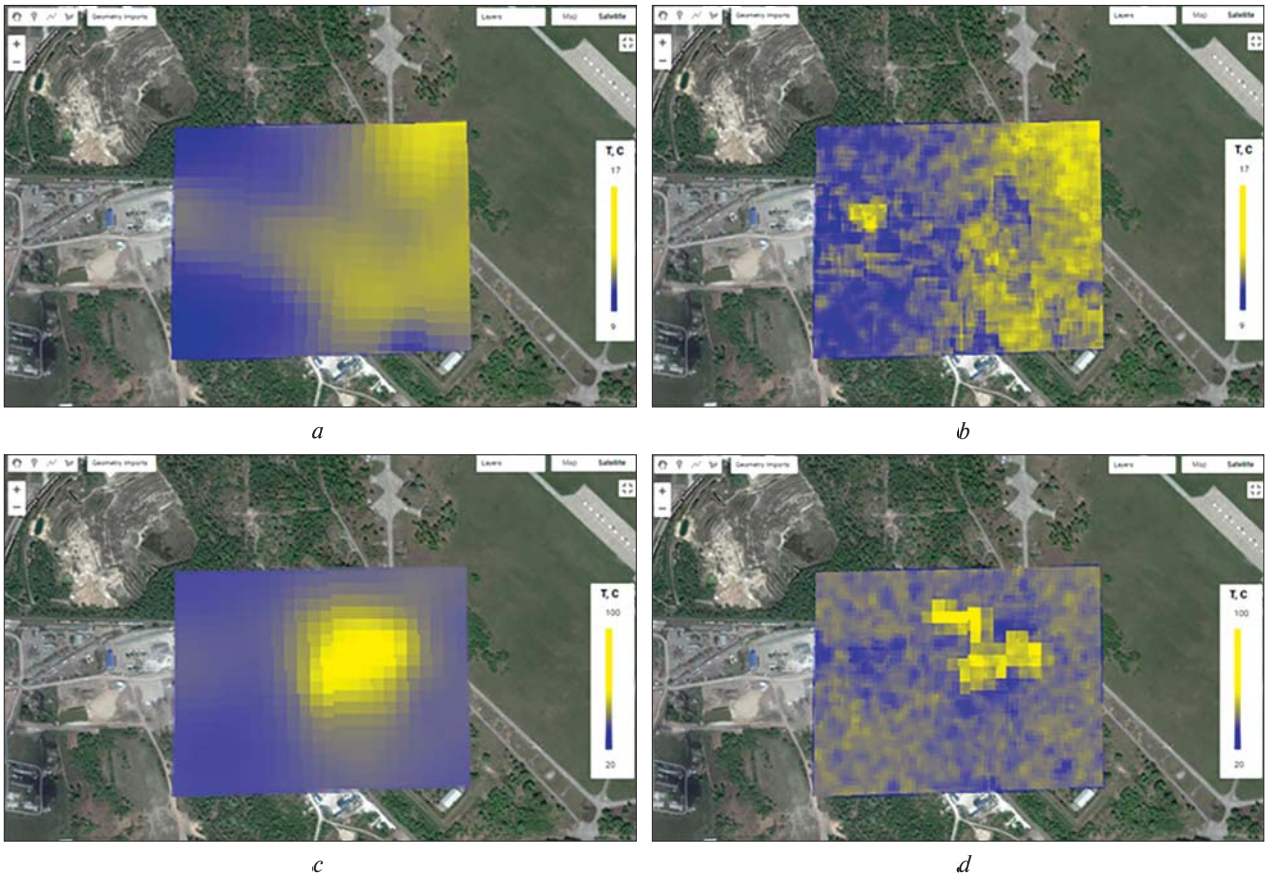

a *b*

c *d*

Fig. 1, a is the brightness temperature field raster fragment in the B_{10} channel of Landsat 8 TIRS; *b* is a fragment of the synthesized pseudo-thermal image T_I^{ir} with an increased spatial resolution before the fire; *c, d* are images of the same types as *a*, *b*, respectively, on the fire date 2015.06.09

tinel 1: *VV, VH* — 10 m; Sentinel 2: B_2...B_4, B_8 — 10 m, B_{11}, B_{12} — 20 m; Landsat 8: B_{10} — 100 m.

Fig. 2 shows the spatial resolution enhancement results of the brightness temperature field image (*b*) at the smoldering fire site on the peat land (*a*) near the Svarychiv village, Ivano-Frankivsk region. Fig. 2, *c* shows a fragment of the synthesized pseudo-thermal image T_{II}^{ir} with the enhanced spatial resolution of 10 m according to the regression model (6) based on data from various space systems with different spatial resolutions: Sentinel 1: *VV, VH* — 10 m; Landsat 8: B_6, B_7 — 30 m, B_8 — 15 m. Fig. 2, *d* shows a fragment of the synthesized pseudo-thermal image T_I^{ir} with an increased spatial resolution of 10 m according to the regression model (5) based on data from sensors of various space systems with different spatial resolutions: Sentinel 1: *VV , VH* — 10 m; Sentinel 2: B_2... B_4, B_8 — 10 m, B_{11}, B_{12} — 20 m; Landsat 8: B_{10} — 100 m.

Fig. 3 presents the results of the spatial resolution enhancement of the brightness temperature field image with the spatial resolution of 100 m of Nyiragongo volcano, Congo (Fig. 3, *b*) and its environs in July 2018, shown in natural colors in Fig. 3, *a*. Fig. 3, *c* shows a fragment of the synthesized pseudo-thermal image T_I^{ir} with the increased spatial resolution of 10 m according to the regression model (5) from sensors of various space systems with different spatial resolutions: Sentinel 1: *VV, VH* — 10 m; Sentinel 2: B2-B4, B_8 — 10 m, B_{11}, B_{12} — 20 m; Landsat 8: B_{10} — 100 m. Fig. 3, *d* shows a fragment of the pseudo-color RGB composite of Landsat 8 data channels: *R* corre-

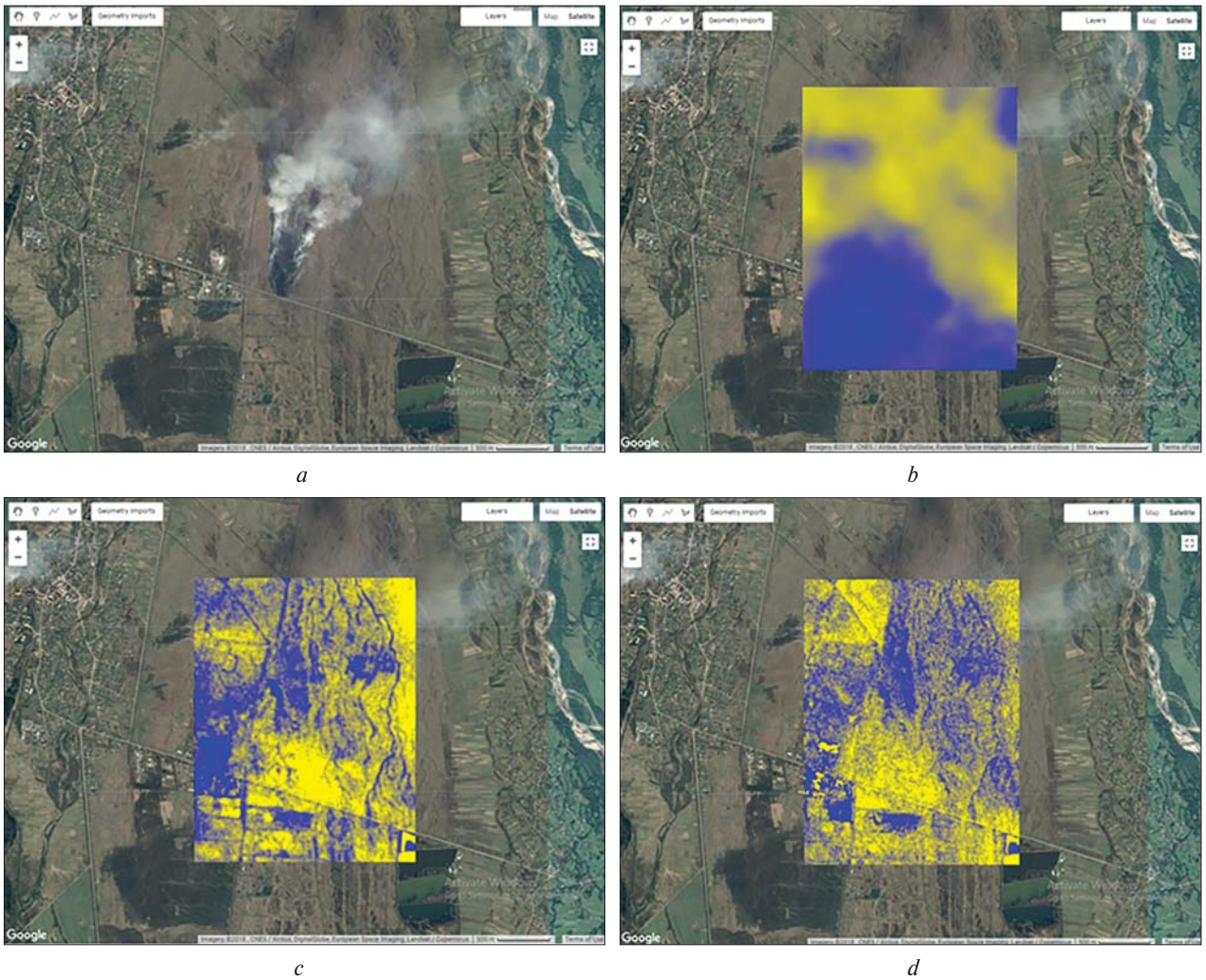

a *b* *c* *d*

Fig. 2, a is the smoldering fire image on the peat land near the Svarychiv v., Ivano-Frankivsk region; *b* is a fragment of the brightness temperature raster in the channel B_{10} Landsat 8 TIRS with the spatial resolution of 100 m; *c* is a fragment of the synthesized pseudo-thermal image T_{II}^{ir} with an increased spatial resolution of 10 m; *d* is a fragment of the synthesized pseudo-thermal image T_{I}^{ir} with an increased spatial resolution of 10 m

sponds to B_6, *G* corresponds to B_7, and *B* corresponds to B_{10}, for which the central wavelengths correspond to the maximum spectral radiance density according to Planck's law for temperatures in the range of 800...1000 K and more, 400...500 K, and 300... 400 K, respectively. The use of this composite illustrates (only approximately and qualitatively) the more contrasting picture of the pixel distribution in the specified temperature ranges in Fig. 3, *d* in comparison with the raster of the synthesized pseudo-thermal image T_{I}^{ir} in Fig. 3, *c*, especially in the volcano crater and on its slopes, albeit with the spatial resolution of 30 m (for qualitative visualization), but not of 10 m, as in the synthesized product.

Synthesis and calibration of the land surface temperature product with the enhanced spatial resolution and daily data providing rate, based on the linear regression on the data from various space systems. The study objective is to implement the developed by authors technology of synthesis and calibration of the land surface temperature product with the enhanced spatial resolution and daily data providing rate based

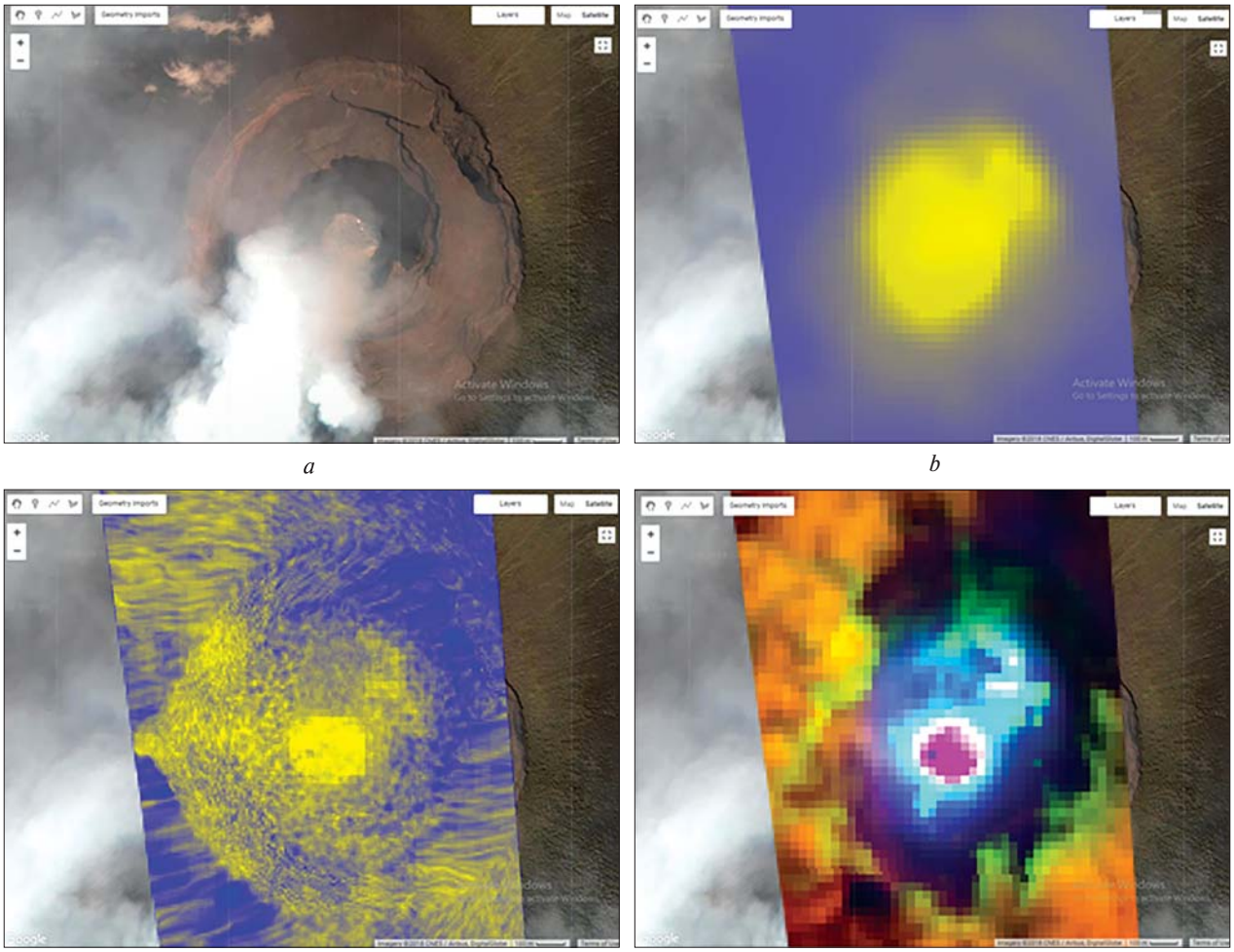

a *b* *c* *d*

Fig. 3, a is a satellite image of the Nyiragongo volcano, Congo, in the natural colors; *b* is a fragment of the brightness temperature raster in the B_{10} Landsat 8 TIRS channel with a spatial resolution of 100 m; *c* is a fragment of the synthesized pseudo-thermal image T_I^{ir} with the enhanced spatial resolution of 10 m; *d* is a fragment of the pseudo-color *RGB* composite of Landsat 8 channels data: *R* corresponds to B_6, *G* corresponds to B_7, *B* corresponds to B_{10}

on the brightness temperature product in the B_{10} channel of the Landsat 8 and the linear regression on MODIS, ASTER and the Sentinel 1 products with data providing rate from daily to moderate. The presented technology is based on the method developed by the authors and described in this article above.

Synthesis of the land surface temperature product with a high spatial resolution and a high data providing rate. The synthesis procedure of the land surface temperature product with the enhanced spatial resolution consists in the implementing of the following multiple linear regression dependence of the land surface temperature image on the test site, selected for further calibration of the synthesized product from averaged in certain time intervals input images in the short-wave infrared, thermal, and radar ranges:

$$U^{cl} = a_0 + a_1 \cdot VV + a_2 \cdot VH + a_3 \cdot B_{07} + a_4 \cdot B_{08} + \\ + a_5 \cdot B_{09} + a_6 \cdot B_{13} + a_7 \cdot B_{14} + a_8 \cdot LST_{Day\_1km}, \quad (7)$$

where U^{cl} is the output synthesized land surface temperature image with the enhanced spatial resolution; a_i $(i = 0,8)$ are scalar coefficients determined by the least squares method; B_{07}, B_{08}, B_{09}, B_{13}, B_{14} are input images of the test site in the respective ASTER bands;

LST_{Day_1km} is the input image of the MOD11A1 product for test site.

The averaging time of the input images in (7) is chosen taking into account the acquisition of at least one qualitative reference image in the averaging period (received once every 16 days) from the Landsat 8 collection: "LANDSAT/LC08/C01/T1_RT" (i. e., the product of thermal infrared channel B10, converted into brightness temperature).

The procedure for synthesizing the land surface temperature product with the enhanced spatial resolution based on the linear regression equation (7) is implemented using the classifier ee.Reducer.linearRegression() [5, 6] on the Google Earth Engine cloud platform.

Calibration of the land surface temperature product with the enhanced spatial resolution. The calibration of the product is performed for the selected test site according to the calibration equation:

$$U^k = (U^{cl} - \text{mean}(U^{cl})) \cdot STD^{kal} / STD^{cl} + \text{mean}(U^{kal}), \quad (8)$$

where U_k is the calibrated land surface temperature product with the enhanced spatial resolution; U^{kal} is reference image in the B_{10} band of Landsat 8, converted to brightness temperature; $\text{mean}(U_{cl})$ and $\text{mean}(U^{kal})$ are average values of U^{cl} and U^{kal}, respectively; STD^{cl}, STD^{kal} are standard deviations of U^{cl} and U^{kal}, respectively.

To estimate the calibration relative error according to the calibration equation (8) for the area of the synthesized image of the land surface temperature with the enhanced spatial resolution, which coincides with the area of the reference image in the B_{10} band of Landsat 8 converted to brightness temperature, the following dependence is used:

$$\varepsilon = \left(\sqrt{\sum_{i\,j} (U_{ij}^k - U_{ij}^{kal})^2} \Big/ \sum_{i\,j} U_{ij}^{kal} \right) \cdot 100,$$

where ε is the calibration relative error in %, which is the relative root mean square error of the synthesized pseudo-thermal image in regard to the reference image for the test site; U_{ij}^k is the brightness temperature value of the pixel of the synthesized image with the enhanced spatial resolution; U_{ij}^{kal} is the brightness temperature value of the image pixel, which is obtained by resampling the reference image with a low spatial resolution to the sampling grid of the synthesized image.

The technology has been developed for synthesis and calibration of the land surface temperature product with the enhanced spatial resolution and daily data providing rate based on the brightness temperature product in the B_{10} band of Landsat 8 and the linear regression on the MODIS, ASTER, and Sentinel 1 products with data providing rate from daily to moderate. JavaScript software has been developed, and the technology was implemented in the form of an interactive web service with open access on the Google Earth Engine Apps cloud platform [6].

Initial data for regression processing according to the developed technology:

- thermal data with a low spatial resolution of 1000 m with a high data providing rate (daily) from the TERRA/MODIS collection "MODIS/006/MOD11A1", i. e., the product "LST_{Day_1km}";
- thermal data with the spatial resolution of 30 (90) m with a high data providing rate from the TERRA/ASTER collection "ASTER/AST_L1T_003", i. e., products of bands B_{07}, B_{08}, B_{09}, B_{13}, B_{14};
- radar data with a high spatial resolution of 10 m with moderate data providing rate (2 days) from the Sentinel 1 collection "COPERNICUS/S1_GRD", i. e., products of *VV, VH* bands.

Initial data for cross-calibration of synthesized thermal images:

- thermal data with the spatial resolution 30 (100) m with a low data providing rate (1 time in 16 days) (reference values) from the Landsat 8 collection "LANDSAT/LC08/C01/T1_RT", i. e., the product of the thermal infrared channel B_{10}, converted into brightness temperature;
- the product of the land surface temperature with the enhanced spatial resolution of 10 m, synthesized as a result of regression processing on satellite data of the thermal and radar ranges.

Observation objects and events:

object 1: "BRSM-Nafta" petroleum company's storage depot, fire, Vasylkiv district of Kyiv region, Ukraine;

object 2: Nyiragongo volcano, eruption, Congo;

object 3: peat lands, fire, Lielsalas hamlet, Latvia.

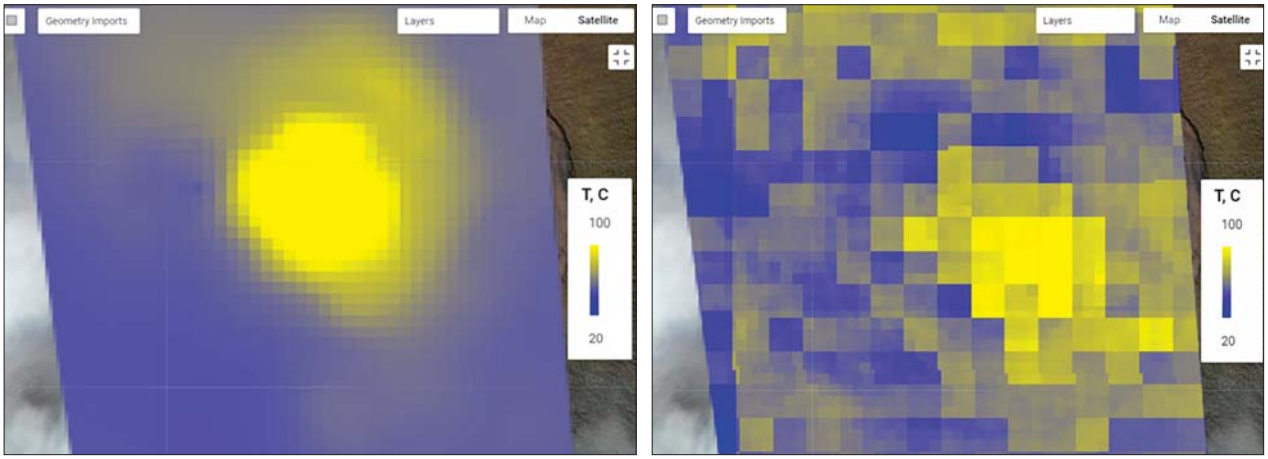

a *b*

Fig. 4, a is a reference image of the brightness temperature for object 2 in the month when the eruption occurred; *b* is the synthesized image of the brightness temperature with the enhanced spatial resolution for object 2 in the same month

Technology implementation examples for synthesis and calibration of thermal imagery with the enhanced spatial resolution. The technology implementation results are presented in the examples of the three observation objects mentioned above.

Object 1. Data processing period: every month from the 3rd to the 10th month of the year during 2015—2019.

The values of the calibration parameters for the test site in the period of the fire 06.2015, when, in fact, the calibration took place, are as follows:

$$\text{mean}(U^{cl}) = 3.9\,,$$

$$\text{mean}(U^{kal}) = 23.37\,,$$

$$STD^{cl} = 0.075\,,$$

$$STD^{kal} = 6.47.$$

The reference image of the brightness temperature for object 1 in the B_{10} band of Landsat 8 TIRS in the period of the fire (06.2015) is shown in Fig. 1, *c*. The synthesized image of the brightness temperature with the enhanced spatial resolution for object 1 in the same period (06.2015) is shown in Fig. 1, *d*.

The calibration relative errors of synthesized thermal images with the enhanced spatial resolution for object 1 according to Landsat 8 reference data for each month from the 3rd to the 10th month of the year during 2015—2019 are shown in Table 1. The table cell with the value of the calibration relative error in the month when there was a fire (06.2015) is shaded.

Table 1. **The calibration relative errors of synthesized thermal images with the enhanced spatial resolution for object 1**

Object 1. Calibration relative errors (%) during 2015—2019					Month
2019	2018	2017	2016	2015	
0.7063	0.8149	0.2413	0.4689	0.8812	3
1.5548	0.588	0.9569	1.1284	2.6089	4
1.3111	N/A	1.8261	1.1685	0.6487	5
1.0723	1.5007	0.6926	1.9351	17.791	6
3.5248	4.2234	3.9182	1.7067	2.7682	7
1.0723	1.5007	0.6926	1.9351	1.4039	8
0.9195	0.5382	0.9581	1.1861	0.7194	9
1.3867	0.5672	N/A	2.4402	6.2002	10

Object 2. Data processing period: every month from the 3rd to the 10th month of the year during 2015—2019. The reference image of the brightness temperature for object 2 in the B_{10} band of Landsat 8 TIRS in the month when the eruption occurred is shown in Fig. 4, *a*. The synthesized image of the brightness temperature with the enhanced spatial resolution for object 2 in the same month is shown in Fig. 4, *b*.

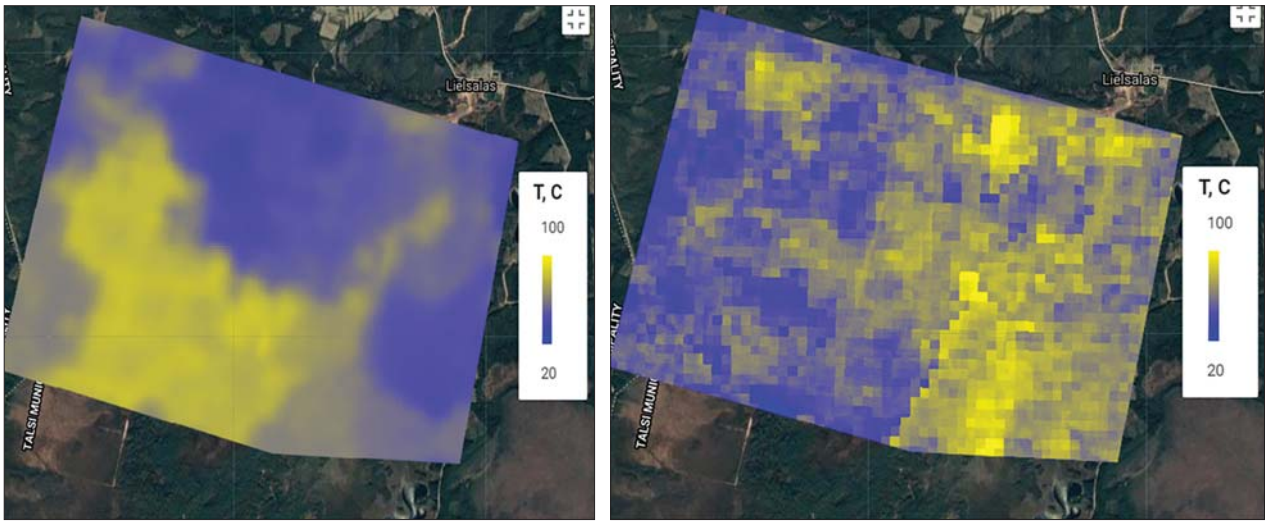

a *b*

Fig. 5*, a* is a reference image of the brightness temperature for object 3 in the month when a fire occurred; *b* is the synthesized image of the brightness temperature with the enhanced spatial resolution for object 3 in the same month

Table 2. **The calibration relative errors of synthesized thermal images with the enhanced spatial resolution for object 2**

Object 2. Calibration relative errors (%) during 2015—2019					Month
2019	2018	2017	2016	2015	
22.098	N/A	10.006	N/A	N/A	3
24.545	N/A	7.4642	N/A	5.6631	4
6.7206	7.3593	1.9849	N/A	N/A	5
18.683	19.406	19.456	19.713	N/A	6
9.2359	28.641	15.382	20.933	N/A	7
N/A	23.893	0.7421	N/A	N/A	8
N/A	6.5604	5.0509	N/A	N/A	9
3.2477	N/A	6.8493	12.934	N/A	10

Table 3. **The calibration relative errors of synthesized thermal images with the enhanced spatial resolution for object 3**

Object 3. Calibration relative errors (%) during 2015—2019					Month
2019	2018	2017	2016	2015	
3.8223	1.1401	N/A	N/A	0.787	3
0.9635	N/A	1.2639	6.2847	1.5476	4
5.1849	2.49	3.6493	N/A	2.3367	5
5.9758	6.1656	7.8078	6.8849	3.1143	6
5.2526	7.6831	1.5783	3.447	3.1671	7
N/A	3.6796	3.4222	2.7019	N/A	8
2.2372	2.6767	N/A	N/A	2.1915	9
1.6414	2.7593	N/A	N/A	2.1534	10

The calibration relative errors of synthesized thermal images with the enhanced spatial resolution for object 2 according to Landsat 8 reference data for each month from the 3rd to the 10th month of the year during 2015—2019 are shown in Table 2. The table cells with values of the calibration relative error in the months when the volcano erupted are shaded.

Object 3. Data processing period: every month from the 3rd to the 10th month of the year during 2015—2019.

The reference image of the brightness temperature for object 3 in the B_{10} band of Landsat 8 TIRS in the month of the fire (07.2018) is shown in Fig. 5, *a*. The synthesized image of the brightness temperature with the enhanced spatial resolution for object 3 in the same month (07.2018) is shown in Fig. 5, *b*.

The calibration relative errors of synthesized thermal images with the enhanced spatial resolution for object 3 according to Landsat 8 reference data for each month from the 3rd to the 10th month of the

year during 2015—2019 are shown in Table 3. The table cell with the value of the calibration relative error in the month when there was a fire (07.2018) is shaded.

CONCLUSIONS

The methodology has been developed for the enhancement of the spatial resolution of the land surface thermal field satellite imagery based on the following steps: coupling images in the visible, thermal, and radar ranges into the single multispectral data product; constructing regression models of the images' relationship; performing the linear regression of the pseudo-thermal product with the enhanced spatial resolution on the visible and radar ranges data. The methodology is implemented on the Google Earth Engine open cloud platform using the Earth Engine API and the software scripts created in the JavaScript language with the processing of multispectral image collections of various space systems at specified time intervals.

The possibility of practical synthesis of the pseudo-thermal image with the enhanced spatial resolution of 10 m based on the thermal image with the resolution of 100 m and the multispectral composite with the layers resolutions of 10 m and 30 m is shown.

Extending the scope of the developed methodology to monitoring high-temperature objects with internal heating sources (fires, geothermal phenomena, etc.) requires further research in the direction of the joint use of the Landsat 8 data in the infrared bands B_6, B_7, and B_{10}. Calibration methods of proposed regression mathematical models and validation of the synthesized thermal images with the enhanced spatial resolution require further development and research.

The technology has been developed for synthesis and calibration of the land surface temperature product with the enhanced spatial resolution and daily data providing rate based on the brightness temperature product in the B10 band of Landsat 8 and linear regression on the MODIS, ASTER, and Sentinel 1 products with data providing rate from daily to moderate one. The software in JavaScript has been developed, and technology in the interactive web service form with open access on the Google Earth Engine Apps cloud platform has been implemented.

The final data product provides the satisfactory relative root mean square error of the brightness temperature recovery of not more than 6 % according to the reference cross-calibration data of the B10 Landsat 8 band in the moderate thermal field (up to 100 °C). The relative root mean square errors of the synthesized data according to the reference data on high-temperature sites (fire, hot lava) up to 28 % are due to the fact that the synthesized product contains information from high-temperature spectral bands (B_7...B_{09} from ASTER), while the reference product (B10 from Landsat 8) does not contain such information.

Technology implementation examples show that cross-calibration of the synthesized product can be performed during the year from March to October according to reference thermal images of natural or artificial objects. Objects selected for calibration must have stable thermal characteristics at the time of satellite flight during the data acquisition period.

REFERENCES

1. *Google Earth Engine Apps. Thermal Images Processing to get 10 m Spatial Resolution by S1, L8 Data Regression*. Developed by S. Chornyy, JS Code 1. URL: https://svch1mail.users.earthengine.app/view/thermal-images-of-10m-resolution (Last accessed: 01.06.2022).
2. *Google Earth Engine. Linear Regression*. URL: https://developers.google.com/earth-engine/guides/reducers_regression (Last accessed: 01.06.2022).
3. Stankevich S. A., Filipovich V. E., Lubsky M. S., Krylova A. B., Kritsuk S. G., Brovkina O. V., Gornyy V. I., Tronin A. A. (2015). Intercalibration of methods for the land surface thermodynamic temperature retrieving inside urban area by thermal infrared satellite imaging. *Ukr. J. Remote Sensing*, № 7, 12—21. URL: http://ujrs.org.ua/ujrs/article/view/59/77 (Last accessed: 01.06.2022) [In Russian].
4. Zyelyk Ya., Chornyy S., Pidgorodetska L. (2017). Mathematical models of the joint calibration process and optimal filtration of integrated multispectral data products of space Earth observations in visible, thermal and radio spectral bands. Abstracts of the 17th Ukrainian Conference on Space Research (Odesa, August, 21—25), 195.

5. Zyelyk Ya. I., Pidgorodetska L. V., Chornyy S. V. (2018). Estimation of the thermodynamic temperature field of the land surface using satellite data based on land cover classification. *Astron. School's Report*, **14,** № 2, 70—77. DOI: https://doi.org/10.18372/2411-6602.14.10 [in Ukrainian].
6. Zyelyk Ya. I., Podgorodetskaya L. V., Chornyy S. V. (2019). Estimation of the thermodynamic temperature of the Earth's surface using satellite data based on the land cover classification in the optical radiation range. *J. Automat. and Inform. Sci.*, **51**, I. 6, 25—40. DOI: 10.1615/jautomatinfscien.v51.i6.30.

Стаття надійшла до редакції 09.06.2022 *Received 09.06.2022*
Після доопрацювання 09.06.2022 *Revised 09.06.2022*
Прийнято до друку 02.08.2022 *Accepted 02.08.2022*

Я. І. Зєлик, голов. наук. співроб., д-р техн. наук., старш. наук. співроб.
С. В. Чорний, старш. наук. співроб., канд. техн. наук, доц.
О. П. Федоров, дир., зав. відділу, д-р фіз.-мат. наук, член-кор. НАН України.
Заслужений діяч науки і техніки України, Лауреат Державної премії України у галузі науки і техніки,
дійсний член Міжнародної академії астронавтики
Л. В. Підгородецька, старш. наук. співроб., канд. техн. наук
E-mail: pidgorodetska@ukr.net
Л. М. Колос, старш. наук. співроб., канд. техн. наук

Інститут космічних досліджень Національної академії наук України та Державного космічного агентства України
Проспект Академіка Глушкова 40, корп. 4/1, Київ, Україна, 03187

ПІДВИЩЕННЯ ПРОСТОРОВОЇ РОЗДІЛЬНОЇ ЗДАТНОСТІ ЗОБРАЖЕНЬ ТЕПЛОВОГО ПОЛЯ ЗЕМНОЇ ПОВЕРХНІ НА ОСНОВІ МОДЕЛЕЙ МНОЖИННОЇ РЕГРЕСІЇ НА БАГАТОСПЕКТРАЛЬНИХ ДАНИХ ВІД РІЗНИХ КОСМІЧНИХ СИСТЕМ

Розроблено методологію підвищення просторової роздільної здатності супутникових зображень теплового поля земної поверхні на основі поєднання зображень у видимому, тепловому та радіолокаційному діапазонах у єдиний багатоспектральний продукт даних; побудови регресійних моделей взаємозв'язку зображень; виконання лінійної регресії псевдотеплового продукту з підвищеною просторовою роздільною здатністю на даних видимого та радіолокаційного діапазонів. Методологію реалізовано на відкритій хмарній платформі Google Earth Engine з використанням Earth Engine API та програмних скриптів, створених мовою JavaScript, з обробкою багатоспектральних колекцій зображень різних космічних систем на заданих часових інтервалах.

Показано можливість практичного синтезу псевдотеплового зображення з підвищеною просторовою роздільною здатністю 10 м на основі теплового зображення з роздільною здатністю 100 м та багатоспектрального композиту з роздільною здатністю шарів 10 і 30 м.

Розроблено технологію синтезу та калібрування продукту температури земної поверхні з підвищеною просторовою роздільною здатністю і темпом надання даних щодня на основі продукту радіаційної температури у каналі B10 «Ландсат-8» та лінійної регресії на продуктах MODIS, ASTER і «Сентінель-1» з темпом надання даних від щоденного до помірного. Розроблено програмне забезпечення на JavaScript та реалізовано технологію у формі інтерактивного вебсервісу з відкритим доступом на хмарній платформі Google Earth Engine Apps.

Кінцевий продукт даних забезпечує задовільну відносну середню квадратичну похибку відновлення радіаційної температури не більше 6 % згідно з прототипами на помірному тепловому полі (до 100 °C) з перехресним калібруванням за зразковими даними «Ландсат-8». Відносні середні квадратичні помилки синтезованих даних згідно із зразковими даними на високотемпературних ділянках (пожежа, розпечена лава) до 28 % зумовлені тим, що синтезований продукт містить інформацію з високотемпературних спектральних каналів (B_7...B_{09} — ASTER), а зразковий продукт (B_{10} — «Ландсат-8») такої інформації не містить.

Приклади застосування технології демонструють, що перехресне калібрування синтезованого продукту можна здійснювати протягом року з березня по жовтень за зразковими тепловими зображеннями природних чи штучних об'єктів. Об'єкти, відібрані для калібрування, повинні мати стабільні теплові характеристики на момент польоту супутників протягом періоду збору даних.

Ключові слова: температура земної поверхні, радіаційна температура, просторова роздільна здатність зображень, множинна лінійна регресія, поєднання різнорідних багатоспектральних даних, темп надання даних, перехресне калібрування продукту, Google Earth Engine.